IEEE Access
Multidisciplinary ⋮ Rapid Review ⋮ Open Access Journal

Received 1 April 2024, accepted 6 May 2024, date of publication 9 May 2024, date of current version 17 May 2024.

Digital Object Identifier 10.1109/ACCESS.2024.3399213

RESEARCH ARTICLE

A Compact Magneto-Electric Dipole Antenna for S-Band MIMO Through-Wall Radar

CHAO SUN[1], NAIKE DU[1], (Member, IEEE), YUCHAO GUO[1], XINHUI ZHANG[1], (Member, IEEE), HUI ZHANG[2], AND XIUZHU YE[1], (Senior Member, IEEE)

[1]School of Information and Electronics Engineering, Beijing Institute of Technology, Beijing 100081, China
[2]School of Integrated Circuit Science and Engineering, Beihang University, Beijing 100191, China

Corresponding author: Xiuzhu Ye (xiuzhuye@outlook.com)

This work was supported in part by the National Natural Science Foundation of China under Grant 61971036, in part by the Fundamental Research Funds for the Central Universities under Grant 2023CX01011, and in part by Beijing Nova Program under Grant 20230484361.

ABSTRACT In order to achieve sufficient penetration depth, the antennas for through-wall radar require low operating frequency, small size, and high gain. In this paper, an ultra-wideband and low-cost magneto-electric (ME) dipole antenna operating in the S-band for through-wall radar application is proposed. A size reduction structure is achieved by proposing a Minkowski-like fractal ground in conjunction with a folded shorted patch to increase the path of the surface equivalent current. Moreover, this structure can be easily machined using multilayer printed circuit board (PCB) with low cost. Test results show that the final prototype has an impedance bandwidth of 66.7% in the frequency range of $1.7 \sim 3.4$ GHz and the peak gain in the frequency range is 7.73 dBi, while maintaining a stable radiation pattern across its entire frequency band. The antenna features a wide bandwidth, compact design, high gain, and low cost, making it suitable for the demanding through-wall applications. The performance of the antenna is compared with the state-of-the-art works to demonstrate its key advantages over similar designs. Additionally, it has been seamlessly integrated into a Frequency Modulation Continuous Wave (FMCW) radar system, where it has undergone practical testing and achieved outstanding detection performance.

INDEX TERMS FMCW system, magneto-electric dipole antenna, MIMO array, miniature antenna, ultra-wideband through-wall radar (TWR).

I. INTRODUCTION

Currently, the promising application potential of through-wall radar sensors has attracted considerable scholarly attention. In the fields of security and disaster rescue, through-wall radar can detect the existence and position of human bodies behind obstacles [1], [2], [3], [4]. Moreover, they can be used for non-contact and non-line-of-sight detection of vital signs (such as heartbeat and breathing) [5], [6], [7], [8]. To acquire multi-dimensional information, most radar sensors necessitate the utilization of multiple-input-multiple-output (MIMO) antenna arrays [9]. Achieving penetration capability necessitates the radar's operation at low frequencies, while high-resolution performance demands a wide frequency band. In through-wall scenarios, signals weaken significantly after wall penetration, necessitating the antennas with high gain performance. Concurrently, there is a substantial need for the system to be miniaturized, ensuring it remains compact and easily portable for individual use. As the initial stage in radar development, the creation of a miniaturized, ultra-wideband, and high-gain antenna design is critical. Meeting all these requirements simultaneously presents significant challenges in antenna design.

There have been several design attempts to the antenna for through-wall radar. Such as in [10], the Vivaldi antenna is employed, and in [11] a log-periodic antenna is adopted, however both of which are too large to form into arrays and have limited application scenarios. In [12], the Archimedean

The associate editor coordinating the review of this manuscript and approving it for publication was Muhammad Usman Afzal.

spiral antenna array is adopted, however with a strong back radiation, which reduced the radiation energy in the front direction.

Compared to the above designs, magneto-electric (ME) dipole antennas have superior characteristics, such as omni-directionality, high gain, small size, and ultra-wide band, which have been widely used in various applications, including base station for mobile communications, ultra-wideband systems, and millimeter-wave applications [13], [14], [15], etc. However, the complex manufacturing process and high cost have limited the usage of ME dipole antennas. In recent years, many scholars have proposed enhanced designs to expand the applicability of the ME dipole antennas. In [16], a C-band ME dipole antenna is developed using multilayer printed circuit board (PCB) technology and H-shaped ground structure, which significantly simplifies the machining complexity and improves the antenna performance. In [17] and [18], dielectric loading and folded parallel-wall structures are applied to reduce the profile of antenna, but they have brought difficulty to the manufacturing process.

This study proposes an ME dipole antenna operating in the S-band, designed to meet the comprehensive needs of through-wall radar applications. Our goal is to refine the design for practical engineering production, effectively overcoming the previously mentioned challenges. The main contributions of this work are summarized as follows: 1) We introduce a novel antenna design that diverges from the traditional folded parallel-wall structure. Utilizing short patches and metal vias on a multi-layer FR4 substrate with high permittivity, this design achieves a low-profile and facilitates ease of fabrication. 2) Specifically, we propose a Minkowski-like fractal ground design that substantially lengthens the equivalent current path of the magnetic dipole. This innovation allows fora reduction in antenna size without compromising its operational frequency. 3) Experimental results reveal that the antenna has an impedance bandwidth of 66.7% within the 1.7 to 3.4 GHz frequency range, while also maintaining a stable radiation pattern throughout its bandwidth. Ultimately, this research culminates in the development of an ultra-wideband, miniaturized, cost-effective, and high-gain antenna, optimized for S-band through-wall radar sensors.

II. DESIGN AND SIMULATION OF ANTENNA

A. PRINCIPLE OF ME DIPOLE ANTENNA

A classical magneto-electric (ME) dipole antenna is achievable through a vertically oriented quarter-wave patch connected to a planar dipole, as depicted in Fig. 1(a). The lower resonance frequency is determined by the length of the electric dipole, whereas the higher resonance frequency depends on the length of the magnetic dipole. Employing a bow-tie shaped planar structure enhances the broadband capabilities of the electric dipole, permitting the adjustment of the operational frequency band by altering the lengths of both dipoles. When both electric and magnetic dipoles are excited with

TABLE 1. Comparison of designed antennas.

Antenna	Bandwidth (GHz)	Gain (dBi)	Dimensions L×W×H(mm^3)
Classical ME dipole	1.25	7.78	120×120×30
Antenna 1	1.42	4.4	60×60×14
Antenna 2	1.57	4.68	60×60×11.2
Antenna 3	1.84	4.92	60×40×8

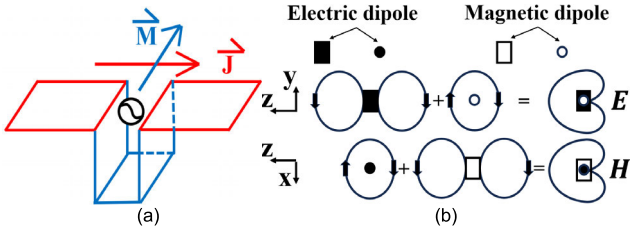

FIGURE 1. Structure of ME dipole antenna, (a) an electric dipole and a quarter-wave patch, (b) principle of radiation pattern formation.

equal amplitude and in phase, the resultant radiation pattern resembles a rotationally symmetric heart shape, consistent across both the E and H planes, and effectively minimizes backward radiation, as illustrated in Fig. 1(b). The ME dipole antenna design is noted for its simplicity and ability to support wideband applications. However, its traditional metal structure poses fabrication challenges, is cost-intensive, and has a comparatively high profile.

B. MINIATURIZATION DESIGN OF PROPOSED ME DIPOLE ANTENNA

As shown in Fig. 2(a), a classical ME dipole antenna is constructed with center frequency of 2.5GHz. It comprises a large square metal ground, a metal sheet curved by 90 degrees, and an Γ−shaped feeding line. The overall height of the antenna is one-fourth of the wavelength corresponding to the center frequency, that is 30mm. The metal structure is quite costly and challenging to fabricate. Recently, the PCB technology has become highly mature and offers easy processing and miniaturization capabilities for PCB antennas, which provides solution to the aforementioned shortcomings of ME antenna.

This study employs an economically viable FR4 substrate to enhance the antenna performance. Fig. 2(b) shows the implementation of antenna 1 of the same bandwidth using a 14mm thick substrate, and the size is greatly reduced with respect to the air since the relative permittivity of the substrate is 4.4. To replace the vertical metal wall of the magneto-electric dipole within the substrate, a series of vertical metal vias are employed. However, due to impractical engineering constraints arising from numerous metal vias and excessive substrate thickness, the structure is divided into seven PCBs each with a 2mm thickness. Next, an antenna 2 is proposed in order to further reduce the profile, as shown

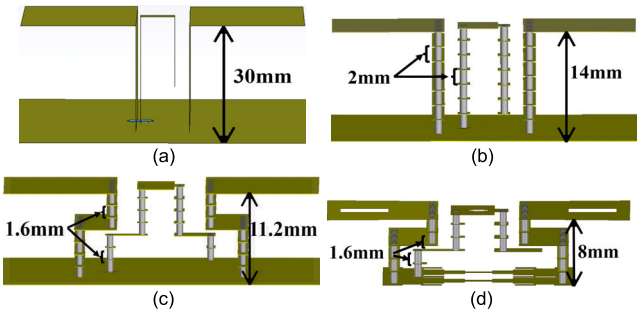

FIGURE 2. (a) Classical ME dipole, (b) antenna 1, (c) antenna 2, (d) antenna 3.

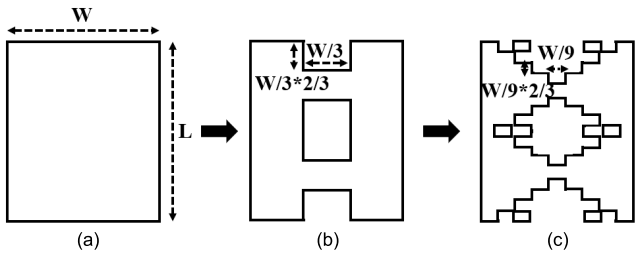

FIGURE 3. (a) 0th-order fractal structure, (b) 1st-order fractal structure, (c) 2nd-order fractal structure.

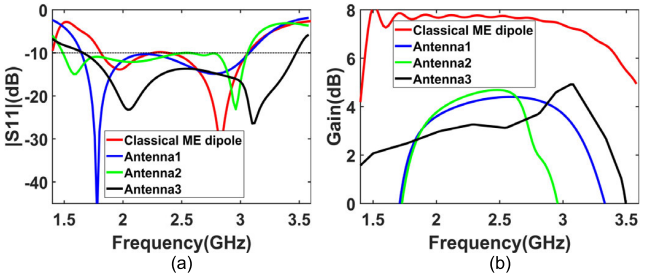

FIGURE 4. Simulation results of the proposed antennas, (a) return loss, (b) gain.

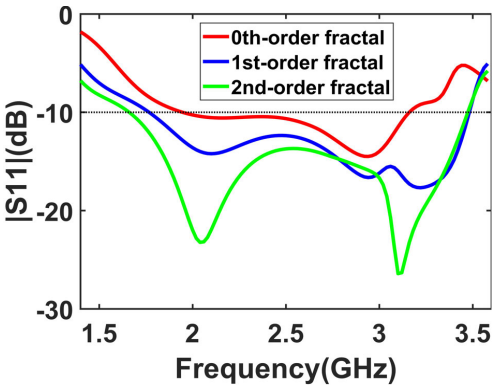

FIGURE 5. Bandwidth at different fractals.

in Fig. 2(c), where the folded vertical metal wall as in [19] is introduced, and a new folded structure is formed by connecting the printed short-circuit patch with the metal vias of each layer, which reduces the profile by 2.8mm on the basis of antenna 1. At this time, it becomes possible to select a thinner (1.6mm) substrate for regulating impedance matching over a wider range. Considering that it is not easy to assemble antenna 2 with too many layers, we propose a structure of Minkowski-like fractal ground to further reduce the height of the profile and finally realize antenna 3 profile with only 0.067 λ. Compared to previous design, antenna 3 is only divided into five layers each with thickness of 1.6 mm.

The iterative process based on the Minkowski-like fractal proposed in this paper is as shown in Fig. 3, where the rectangular floor is divided into two from the long side, and the length of the rectangular floor is set to be L and the width to be W, and the size ratio of the etched rectangle is set to be 2:3. Small rectangles of $W/3 \times W/3*2/3$ are etched out from each wide side to form the 1st-order fractal structure as shown in Fig. 3(b). On this basis, small rectangles of $W/9 \times W/9*2/3$ are etched into the 1st-order fractal structure in the same way to obtain the 2nd-order fractal structure shown in Fig. 3(c). Antenna 3 uses a structure that avoids the coaxial feeding port based on the fractal of 2nd-order.

The implementation of Minkowski fractal theory in antenna design significantly enhances the size and bandwidth of the antenna [20], [21], [22], [23] and the Minkowski-like fractal proposed in this paper is innovative on this basis. On the one hand, the Minkowski fractals proposed by the previous literatures are all based on strict square structure, while this paper extends the fractal to arbitrary rectangular structures. On the other hand, in order to maximize the extension of the current paths, this paper hollows out the middle of the rectangle to realize the fractal in the central part, which doubles the current path as compared to the traditional fractal structures in the literatures.

C. SIMULATION VERIFICATION OF ANTENNA

The simulation results of return loss and gain for the four proposed antennas are given in Fig. 4, and a brief comparison is listed in Table 1, which indicate that antenna 3 has the maximum bandwidth and minimum dimension. Fig. 5 illustrates the return loss of different fractal structures, which demonstrates that higher fractal order ground results in wider bandwidth and better return loss due to the substantial extension of the ground current path. Fig. 6 shows the current distribution for each fractal structure. It is indicated that the 2nd-order Minkowski-like fractal structure concentrates the currents to the central connection point of the ground, which then flow along both inner and outer edges in staircase-like paths. As depicted in Fig. 6(c), there are four ladder-type structures, resulting in an extended path for the currents. Consequently, the resonance frequency of magnetic dipole is shifted towards lower band, which ultimately reduces the height of the magnetic dipole.

In the radar sensor, a metal back shell is placed between the antennas and the transceiver to prevent the radiation from the device [24], [25], [26]. This design allows the metal shell to function as a back reflector for the antenna, thereby reducing

TABLE 2. Detail dimensions of proposed antenna.

Parameters	Value/mm	Parameters	Value/mm
L	40	w3	7.1
W	60	w4	2
l1	37	w5	2
l2	34	w6	1.6
l3	6	w7	6.9
l4	17.6	w8	7.5
l5	34	w9	3
l6	6	R	1.5
l7	3.2	r	0.5
l8	34	r1	0.7
l9	2	h1	1.6
w1	16	h2	8
w2	6.3	h3	20

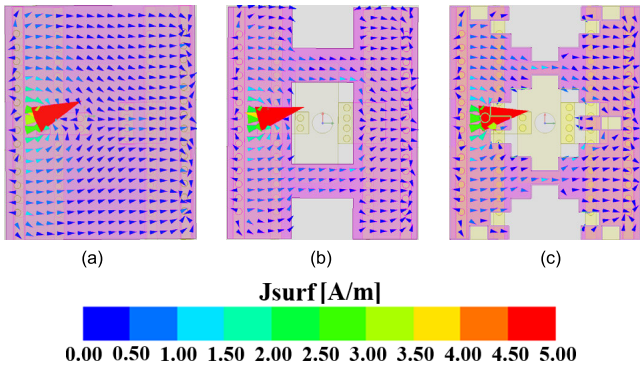

FIGURE 6. Current paths for different fractals, (a) 0th-order fractal, (b) 1st-order fractal, (c) 2nd-order fractal.

back radiation and increasing the gain. In Fig. 7 simulation show that the gain of the antenna can reach 8dBi without affecting the bandwidth when a 100mm ×100mm metal wall is set at 20mm behind the substrate.

III. MEASUREMENT AND ANALYSIS

Fig. 8 illustrates the design details of the antenna. The substrate is chosen as FR4 with relative permittivity of 4.4 and thickness of 1.6 mm. Five layers of substrates and reflector are mechanically fastened with plastic screws to form into the antenna with total thickness of 28 mm.

A. ANTENNA GEOMETRY

The top layer is the electric dipole of bow-tie shape, and the square notches are the locations of the plastic screws. The electric dipole operates at quarter wavelength of the medium. Different layers are connected by the vias, located at the inner side of the bow-tie dipole. Two parallel wall structures are created by the vias and the printed short-circuit patches. Excitation of the antenna is achieved by using a Γ−shaped probe consisted of a T-shaped patch on the top layer and the vias

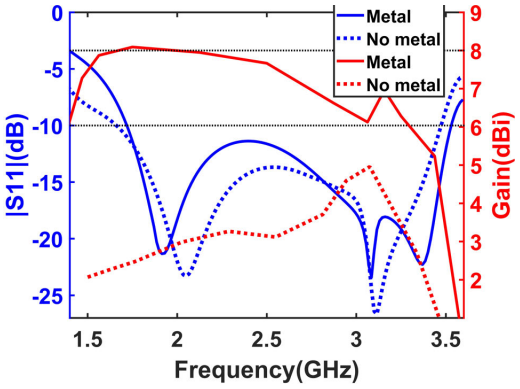

FIGURE 7. Comparison of antenna 3 and the final proposed antenna (effect of metal reflector on antenna performance).

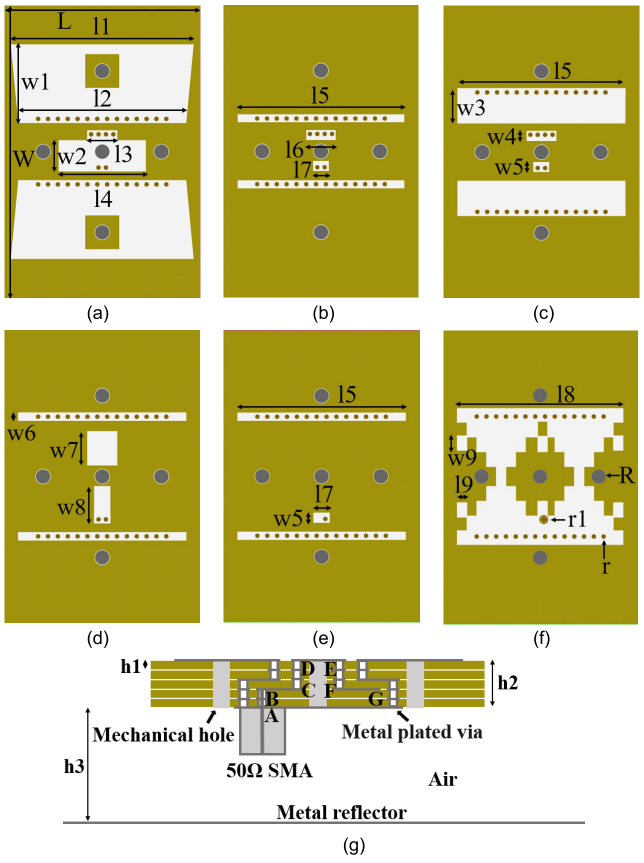

FIGURE 8. Design details of the final proposed antenna, (a) Top layer, (b) second layer, (c) third layer, (d) fourth layer, (e) fifth layer, (f) bottom layer, (g) horizontal cut.

in each layer. The Γ−shaped probe, as shown in Fig. 8(g), consists of vertical vias (sections AB, CD, and EF), printed short-circuit patches (sections BC and FG), and T-shaped patches (section DE). The impedance matching of the antenna is adjusted by the EF and FG sections. The vertical probe is fed by a 50Ω SMA coaxial connector. The SMA internal conductor is inserted into the substrate through section AB, and the external conductor is connected by solder to the

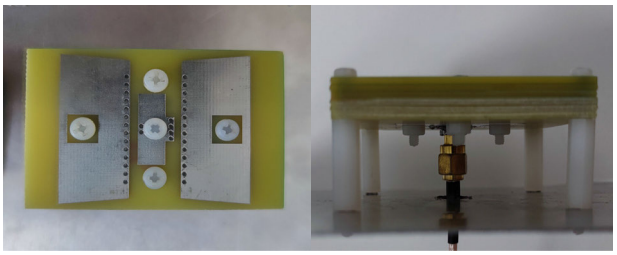

FIGURE 9. A prototype of the antenna.

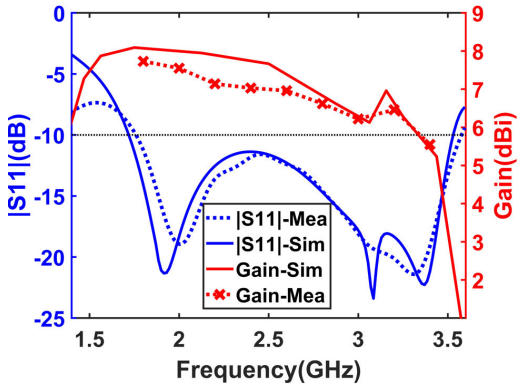

FIGURE 10. Simulated and measured |S11| and gain of the proposed antenna.

Minkowski-like fractal ground. The detailed dimensions of the proposed antenna are as shown in Table 2.

To validate the proposed design, a prototype of the antenna is manufactured as shown in Fig. 9, with an additional back reflector of 100mm ×100mm. The current path of the patch is analyzed to determine the optimal locations for piercing and creating mechanical holes without affecting the radiation characteristics of the antenna. This approach significantly reduces the cost of the antenna to a mere few dollars in average, as no complex machining process is required. Experimental testing involves employing vector network analyzer and a standard microwave anechoic chamber, while simulation is conducted using commercial software HFSS.

B. RETURN LOSS AND GAIN

Fig. 10 illustrates the |S11| and gain of the antenna, indicating that the measured impedance bandwidth covers a wide bandwidth of 66.7% (1.7 GHz ∼3.4 GHz), which is in good agreement with simulation results. The measured in-band gain curve is basically consistent with the simulation trajectory, with a maximum value of 7.73dBi.

C. RADIATION PATTERNS

Three frequency points are selected from the frequency band to analyze the radiation pattern, as illustrated in Fig.11. It is evident that both E-plane and H-plane patterns exhibit a high level of consistency. The measurement data closely aligns with the simulation results. Although the pattern exhibits slight deformation at high frequencies, as evidenced by

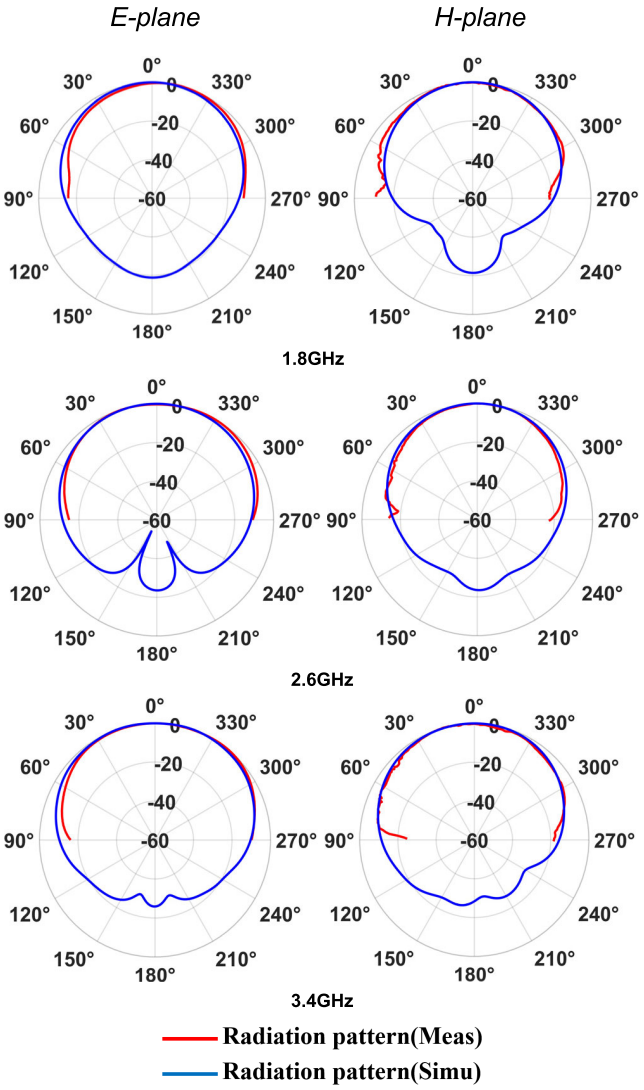

FIGURE 11. Simulated and measured radiation patterns at 1.8, 2.6 and 3.4 GHz.

simulation and measured data, its impact on the system is negligible over a wide range of angles. The actual tested 3dB beamwidth ranges from 70° to 91° in the H-plane and 81° to 105° in the E-plane, which can extend the detection range of our radar system and help the radar sensor to recognize targets at large angles.

D. RADIATION EFFICIENCY

The simulated efficiency of the proposed antenna is shown in Fig. 12. As shown in the figure, the efficiency is ranged between 83% and 93% within the spectrum of the through-wall radar, which indicates the proposed antenna effectively radiated.

E. COMPARISON WITH STATE OF THE ART DESIGNS

Antennas designed for through-wall applications should possess high gain to ensure efficient wave transmission across walls while also have an ultra-wide bandwidth to

TABLE 3. A comparison between different antennas used for through wall radar.

Structure	Reference	Substrate	Center frequency (GHz)	Bandwidth (percent)	Maximum gain (dBi)	Dimension (λ_0^3)	Radiation mode
Monopole	[28]	Ceramic	0.69	75.4	-2.8	0.234×0.234×0.007	Broad-side
Vivaldi	[29]	FR4	1.5	133.3	10.1	1.25×1×0.008	End-fire
Patch-like	[30]	FR4	1.25	120	6.8	0.708×0.583×0.007	End-fire
Vivaldi	[31]	Rogers 4350B	5	40	9	1.833×1.35×0.025	End-fire
Dielectric loaded	[32]	Rogers 4003C	3.3	160	15	3.76×2.44×1.96	End-fire
Microstrip	[33]	FR4	6.6	72.7	8	0.8×0.53×0.255	Broad-side
Bow-tie	[34]	ZYF255DA	1.55	96	4	0.84×0.33×0.215	Broad-side
Proposed antenna		FR4	2.55	66.7	8	0.51×0.34×0.238	Broad-side

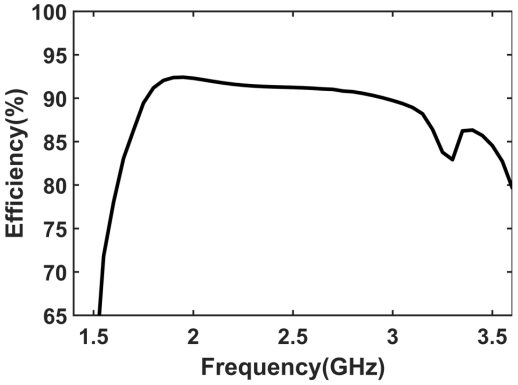

FIGURE 12. Simulated radiation efficiency of proposed antenna versus frequency.

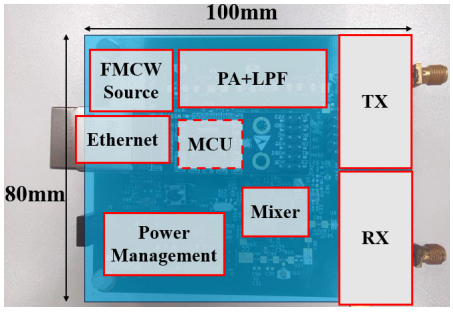

FIGURE 13. FMCW radar system.

improve imaging resolution. The commonly used antennas for through-wall applications include Vivaldi, horn, bow-tie, and microstrip patch antennas [27]. Table 3 presents a comparative analysis encompassing the operational frequency, bandwidth, gain, substrate material, and dimensions of diverse antennas for both proposed and other through-wall antennas in literatures. From Table 3, it can be concluded that Vivaldi antennas typically exhibit considerable gain and an ultra-wideband frequency bandwidth for through-wall radar, however, they are limited by their end-fire nature and large size, which is against the miniature design. On the other hand, although the printed antennas are broad-side with small size, they generally have low gain. In comparison, the proposed antenna has the most economical substrate and smallest size while maintaining high gain and ultra-wideband characteristics, and operates in the most suitable frequency band required for through-wall radar, which is an obvious advantage for miniaturized through-wall radar sensor applications.

IV. RADAR SYSTEM AND EXPERIMENTAL SCENARIOS

A. FMCW RADAR SYSTEM

To comprehensively evaluate the performance of the designed antenna, a frequency modulation continuous wave (FMCW) through-wall radar is developed. The whole system is realized by a printed circuit board with dimension 100mm×80mm, and the overall structure of the system is as shown in Fig. 13. The operating frequency band of the radar is 1.8GHz to 3.2GHz while maintaining a transmit power level of 15dBm.

The operating principle of the FMCW system is as indicated in Fig. 14, which depicts the transmitted signal (TX-chirp) and the received signal (RX-chirp) reflected from an object. It should be noted that the RX-chirp is merely a time-delayed version of the TX chirp, where τ represents the round-trip time between the radar and the object, while S denotes the slope of the chirp waveform. The electromagnetic wave reflected by the object is captured by the antenna, amplified and filtered before being fed into the mixer. The output signal of the mixer is the difference between the TX-chirp and the RX- chirp, as shown in Fig. 14(b), which is a signal with a fixed frequency. Then intermediate frequency signal (IF-signal) can be obtained by Fast Fourier

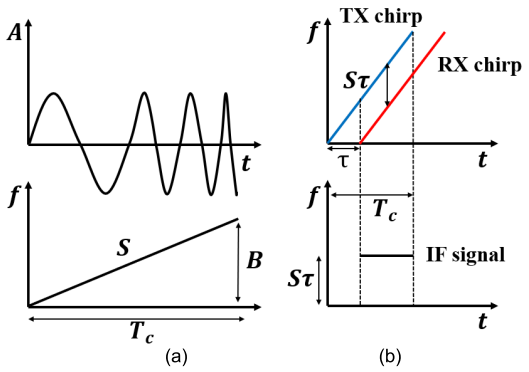

FIGURE 14. Principle of FMCW distance measurement.

Transform (FFT) algorithm after analog-to-digital converter (ADC) acquisition. Finally, utilizing an equation derived below allows us to establish a relationship between IF-signal and distance:

$$c\tau = 2d \tag{1}$$

$$f = S\tau \tag{2}$$

$$f = 2Sd/c \tag{3}$$

where d is the distance from the target to the antenna, and c represents the speed of light.

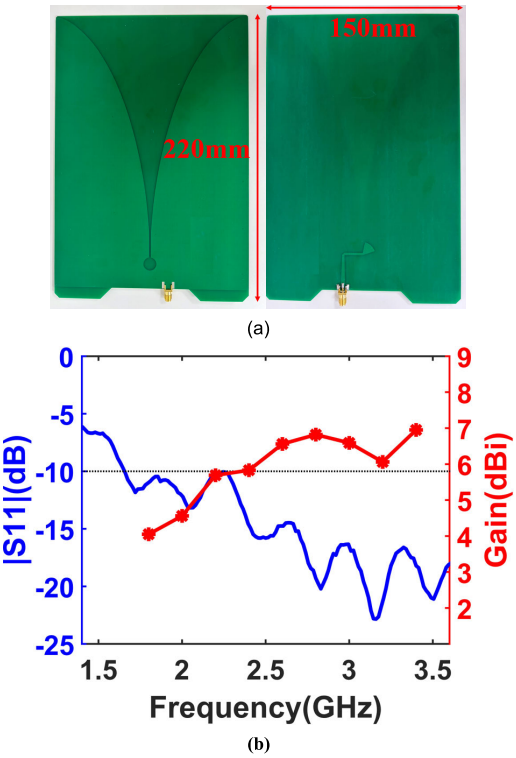

FIGURE 15. (a) The Vivaldi antenna, (b) measured return loss and gain of the Vivaldi antenna.

B. THROUGH-WALL EXPERIMENT

A Vivaldi antenna (since it is mostly used in through wall application) is chosen as comparison to the proposed antenna in through wall experiment. Fig. 15 shows the measured return loss and gain of the Vivaldi antenna. The proposed antenna and Vivaldi antenna are respectively connected to the constructed FMCW radar sensor using 50cm coaxial cable for detecting human targets in complex through wall environments. A subject is involved in the experiment and the consent of this subject has been obtained by a face-to-face interview. The human target walks back and forth for 20 seconds from 2m to 3.5m away from the wall in the house, and the wall is brick and mortar with a thickness of 37cm. A wooden board is placed at 4.5m inside the house to separate the experimental site, with sundries such as cabinets and heaters located behind it. Fig. 16 (a) and (d) show the real scene of the experiment. The distance between the transmitting and receiving antennas is set to 2λ. The Vivaldi antenna is inserted into the foam board to ensure minimal impact on its radiation characteristics, while the antenna proposed in this paper is fixed on the metal reflector.

The comparison results obtained by the two kinds of antennas in identical motion scene are presented in Fig.16. The spectrograms correspond to the squared magnitude of the Fast Fourier Transform (FFT) at each frame are presented, with the horizontal axis representing time and the vertical axis representing the distance. The specific value of the spectrogram allows visualizing the strength of the signal reflected from the target over time at different frequencies, where the colormap represents the received echo power. To highlight the target waveform, we truncate the wall reflection interference within 1m in the spectrogram. Slight mismatches are caused by the multiple reflections from other static objects and the multi-path propagation of the wave, since the experiments are conducted in real world situation instead of an ideal environment like anechoic chamber.

From Figs. 16 (b), (e), it is evident that the static environment used for the experiment is very complex with multiple strong reflectors. However, Fig. 16 (c) and (f) show that when the human target enters the test field and walks back and forth, a significant triangular spectrum is generated by the motion which suppresses the interference caused by the static strong reflectors in the environment. The phenomenon has demonstrated the effectiveness of the proposed through wall radar system. From Fig. 16 (c) and (f), one can see that both the proposed antenna and the Vivaldi antenna are able to find the moving human target, while the proposed ME dipole antenna provides significant higher received power spectrum. Obviously, the performance of our proposed ME dipole antenna surpasses that of the Vivaldi antenna, while significantly improves the miniaturization of the whole radar system.

C. THROUGH-WALL APPLICATION OF MIMO ARRAY

Finally, 2D imaging of through-wall radar with a MIMO array is performed in an empty room to verify the practicality

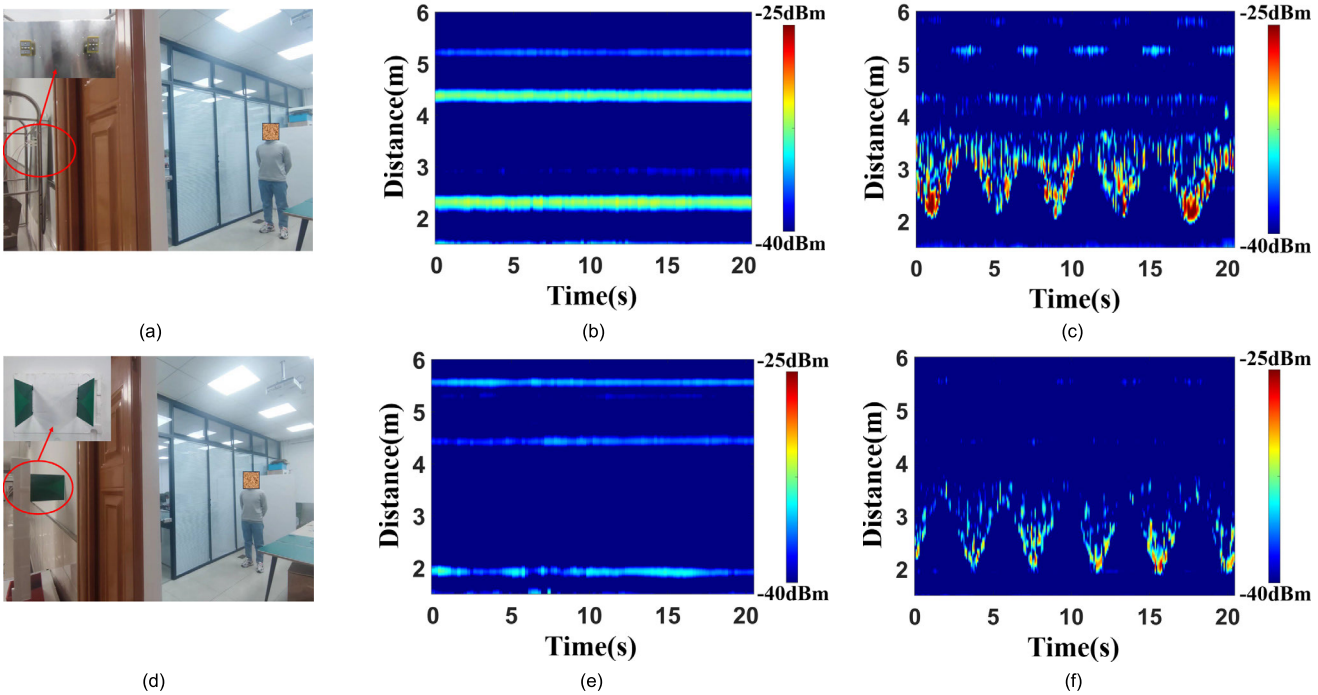

FIGURE 16. Photos of scene from the experimental setup (a),(d), spectrograms of the static environment (b),(e), and spectrograms of the target human (c),(f), where (a),(b),(c) are the proposed antenna and (d),(e),(f) are the Vivaldi antenna.

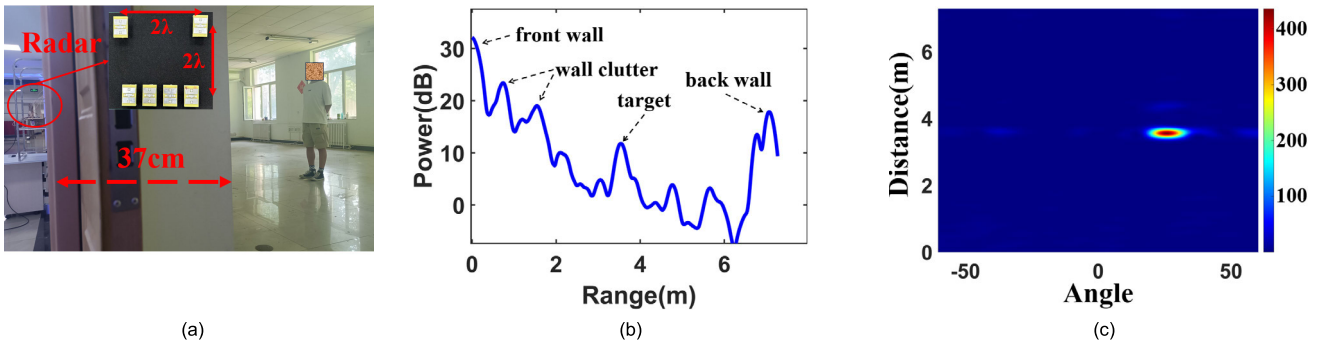

FIGURE 17. FMCW MIMO radar imaging through wall, (a) test conditions, (b) FFT result, (c) 2D imaging result.

and reliability of the antenna. The antenna array is a top-down distributed square array consisting of two transmitting antenna elements and four receiving antenna elements, as shown in Fig. 17(a). Thanks to the miniature size of the proposed antenna, the dimensions of this antenna array are no larger than 40 cm ×40 cm. The antenna array is placed against the wall, which is 37 cm thick and consists of solid bricks, and tested by a person standing 3.5 meters behind the wall at an angle. After applying the 1D Fast Fourier Transform (FFT) algorithm directly to the test data, Fig. 17(b) clearly displays peaks representing the exact location of the human body, while Fig. 17(c) exhibits the final 2D imaging results of the system after the background removal process. These results show that this antenna can be practically applied to a single-person portable MIMO through-wall radar sensor.

V. CONCLUSION

This study introduces a miniaturized, ultra-wideband magneto-electric (ME) dipole antenna designed for S-band through-wall radar applications, achieving a maximum gain of 7.73 dBi and an impedance bandwidth of 66.7%. This design maintains the core advantages of ME antennas, including wide beam coverage, ultra-wideband performance, and high gain, while also achieving significant reductions in fabrication costs and size. A comparative through-wall experiment, conducted against the widely used Vivaldi antenna, demonstrates that the proposed antenna not only delivers a stronger receiver spectrum but also offers superior flexibility for integration into miniature-size MIMO arrays. These characteristics make the proposed antenna highly suitable for MIMO arrays in ultra-wideband, low-frequency radar systems.

REFERENCES

[1] G. W. Kim, S. W. Lee, H. Y. Son, and K. W. Choi, "A study on 3D human pose estimation using through-wall IR-UWB radar and transformer," *IEEE Access*, vol. 11, pp. 15082–15095, 2023.

[2] H. Li, G. Cui, S. Guo, L. Kong, and X. Yang, "Human target detection based on FCN for through-the-wall radar imaging," *IEEE Geosci. Remote Sens. Lett.*, vol. 18, no. 9, pp. 1565–1569, Sep. 2021.

[3] A. Wang, C. Chen, and W. Chen, "Cluster adaptive matching pursuit for multipolarization through-wall radar imaging," *IEEE Sensors J.*, vol. 23, no. 1, pp. 414–424, Jan. 2023.

[4] Z. Zheng, J. Pan, Z. Ni, C. Shi, S. Ye, and G. Fang, "Human posture reconstruction for through-the-wall radar imaging using convolutional neural networks," *IEEE Geosci. Remote Sens. Lett.*, vol. 19, pp. 1–5, 2022.

[5] Z. Ling, W. Zhou, Y. Ren, J. Wang, and L. Guo, "Non-contact heart rate monitoring based on millimeter wave radar," *IEEE Access*, vol. 10, pp. 74033–74044, 2022.

[6] E. Piuzzi, S. Pisa, P. D'Atanasio, and A. Zambotti, "Radar cross section measurements of the human body for UWB radar applications," in *Proc. IEEE Int. Instrum. Meas. Technol. Conf.*, May 2012, pp. 1290–1293.

[7] J. Xiong, H. Hong, H. Zhang, N. Wang, H. Chu, and X. Zhu, "Multitarget respiration detection with adaptive digital beamforming technique based on SIMO radar," *IEEE Trans. Microw. Theory Techn.*, vol. 68, no. 11, pp. 4814–4824, Nov. 2020.

[8] M. Mercuri, I. R. Lorato, Y.-H. Liu, F. Wieringa, C. V. Hoof, and T. Torfs, "Vital-sign monitoring and spatial tracking of multiple people using a contactless radar-based sensor," *Nature Electron.*, vol. 2, no. 6, pp. 252–262, Jun. 2019.

[9] M. Wang, G. Cui, L. Kong, and X. Yang, "First-order rear-wall multipath positioning and suppression for through-wall imaging radar," *IEEE Sensors J.*, vol. 18, no. 20, pp. 8261–8274, Oct. 2018.

[10] R. Cicchetti, S. Pisa, E. Piuzzi, E. Pittella, P. D'Atanasio, and O. Testa, "Numerical and experimental comparison among a new hybrid FT-music technique and existing algorithms for through-the-wall radar imaging," *IEEE Trans. Microw. Theory Techn.*, vol. 69, no. 7, pp. 3372–3387, Jul. 2021.

[11] P.-H. Chen, M. C. Shastry, C.-P. Lai, and R. M. Narayanan, "A portable real-time digital noise radar system for through-the-wall imaging," *IEEE Trans. Geosci. Remote Sens.*, vol. 50, no. 10, pp. 4123–4134, Oct. 2012.

[12] J. Pan, S. Ye, C. Shi, K. Yan, X. Liu, Z. Ni, G. Yang, and G. Fang, "3D imaging of moving targets for ultra-wideband MIMO through-wall radar system," *IET Radar, Sonar Navigat.*, vol. 15, no. 3, pp. 261–273, Mar. 2021.

[13] H. Li, C. Liu, S. Lv, and F. Wu, "Compact magneto-electric dipole array with wide beam scanning range for 5G NR bands," *IEEE Access*, vol. 11, pp. 88489–88497, 2023.

[14] S. Ni, X. Li, X. Qiao, Q. Wang, and J. Zhang, "A compact dual-wideband magnetoelectric dipole antenna for 5G millimeter-wave applications," *IEEE Trans. Antennas Propag.*, vol. 70, no. 10, pp. 9112–9119, Oct. 2022.

[15] J. Xu, W. Hong, Z. H. Jiang, and H. Zhang, "Low-cost millimeter-wave circularly polarized planar integrated magneto-electric dipole and its arrays with low-profile feeding structures," *IEEE Antennas Wireless Propag. Lett.*, vol. 19, pp. 1400–1404, 2020.

[16] H. W. Lai and H. Wong, "Substrate integrated magneto-electric dipole antenna for 5G Wi-Fi," *IEEE Trans. Antennas Propag.*, vol. 63, no. 2, pp. 870–874, Feb. 2015.

[17] L. Siu, H. Wong, and K.-M. Luk, "A dual-polarized magneto-electric dipole with dielectric loading," *IEEE Trans. Antennas Propag.*, vol. 57, no. 3, pp. 616–623, Mar. 2009.

[18] L. Ge and K. M. Luk, "A magneto-electric dipole antenna with low-profile and simple structure," *IEEE Antennas Wireless Propag. Lett.*, vol. 12, pp. 140–142, 2013.

[19] L. Ge and K. M. Luk, "A low-profile magneto-electric dipole antenna," *IEEE Trans. Antennas Propag.*, vol. 60, no. 4, pp. 1684–1689, Apr. 2012.

[20] S. Dhar, R. Ghatak, B. Gupta, and D. R. Poddar, "A wideband Minkowski fractal dielectric resonator antenna," *IEEE Trans. Antennas Propag.*, vol. 61, no. 6, pp. 2895–2903, Jun. 2013.

[21] V. V. Reddy, E. Navyasri, P. Shashidhar, and S. Faize, "Minkowski fractal boundary patch antenna for GPS application," in *Proc. 6th Int. Conf. Commun. Electron. Syst. (ICCES)*, Jul. 2021, pp. 385–388.

[22] E. Ozturk and B. Saka, "Multilayer Minkowski reflectarray antenna with improved phase performance," *IEEE Trans. Antennas Propag.*, vol. 69, no. 12, pp. 8961–8966, Dec. 2021.

[23] L. Zhang, T. F. Eibert, and M. S. Tong, "A self-complementary Minkowski fractal patch antenna for multiband applications," in *Proc. Photon. Electromagn. Res. Symp. (PIERS)*, Jul. 2023, pp. 1354–1360.

[24] Z. Xu, S. Guo, J. Chen, Z. Zhu, S. Xue, P. Wu, G. Cui, and L. Kong, "Multi-domain features-based NLOS target localization method for MIMO UWB radar," *IEEE Sensors J.*, vol. 23, no. 23, pp. 29314–29322, Dec. 2023.

[25] G. Liu, X. Li, C. Xu, L. Ma, and H. Li, "FMCW radar-based human sitting posture detection," *IEEE Access*, vol. 11, pp. 102746–102756, 2023.

[26] Y. Song, T. Jin, Y. Dai, and X. Zhou, "Efficient through-wall human pose reconstruction using UWB MIMO radar," *IEEE Antennas Wireless Propag. Lett.*, vol. 21, pp. 571–575, 2022.

[27] H. Jamshidi-Zarmehri, A. Akbari, M. Labadlia, K. E. Kedze, J. Shaker, G. Xiao, and R. E. Amaya, "A review on through-wall communications: Wall characterization, applications, technologies, and prospects," *IEEE Access*, vol. 11, pp. 127837–127854, 2023.

[28] Y.-J. Ren, C.-P. Lai, P.-H. Chen, and R. M. Narayanan, "Compact ultra-wideband UHF array antenna for through-wall radar applications," *IEEE Antennas Wireless Propag. Lett.*, vol. 8, pp. 1302–1305, 2009.

[29] Z. Hu, Z. Zeng, K. Wang, W. Feng, J. Zhang, Q. Lu, and X. Kang, "Design and analysis of a UWB MIMO radar system with miniaturized Vivaldi antenna for through-wall imaging," *Remote Sens.*, vol. 11, no. 16, p. 1867, Aug. 2019.

[30] F. Fioranelli, S. Salous, I. Ndip, and X. Raimundo, "Through-the-wall detection with gated FMCW signals using optimized patch-like and Vivaldi antennas," *IEEE Trans. Antennas Propag.*, vol. 63, no. 3, pp. 1106–1117, Mar. 2015.

[31] J. Zhang, H. Lan, M. Liu, and Y. Yang, "A handheld nano through-wall radar locating with the gain-enhanced Vivaldi antenna," *IEEE Sensors J.*, vol. 20, no. 8, pp. 4420–4429, Apr. 2020.

[32] R. Cicchetti, V. Cicchetti, A. Faraone, L. Foged, and O. Testa, "A compact high-gain wideband lens Vivaldi antenna for wireless communications and through-the-wall imaging," *IEEE Trans. Antennas Propag.*, vol. 69, no. 6, pp. 3177–3192, Jun. 2021.

[33] T. Hariyadi, Y. T. Huda, and B. Mulyanti, "A small ultra-wideband unidirectional microstrip antenna for through-wall radar application," *J. Telecommun., Electron. Comput. Eng. (JTEC)*, vol. 8, no. 1, pp. 25–28, 2016.

[34] Q. Lu, L. Zhou, C. Tan, and L. Guanghua, "A novel wide beam UWB antenna design for through-the-wall radar," in *Proc. Int. Conf. Microw. Millim. Wave Technol.*, May 2010, pp. 1912–1915.

CHAO SUN received the B.E. degree in electronic information science and technology from Lanzhou University, Lanzhou, China, in 2019. He is currently pursuing the M.S. degree in electronic and information engineering with Beijing Institute of Technology, Beijing, China. His research interests include ultra-wideband radar systems and antenna design.

NAIKE DU (Member, IEEE) received the B.E. degree in electronic and information engineering from the University of Electronic Science and Technology of China, Chengdu, China, in 2016, and the M.S. degree from Waseda University, Japan, in 2018. He is currently pursuing the Ph.D. degree in electronic and information engineering with Beijing Institute of Technology, Beijing, China. His current research interests include inverse scattering problem and biomedical imaging based on deep learning.

YUCHAO GUO received the B.E. degree from Jimei University, Xiamen, China, in 2020. He is currently pursuing the Ph.D. degree with Beijing Institute of Technology, Beijing, China. His current research interests include ultra-wideband radar systems and through-the-wall radar human imaging and motion recognition techniques.

XINHUI ZHANG (Member, IEEE) received the B.S. degree in electromagnetic field and microwave technology from Harbin Institute of Technology (Weihai Campus), Weihai, China, in 2018, and the M.S. degree in electromagnetic field and microwave technology from the University of Electronic Science and Technology of China, Chengdu, China, in 2021. He is currently pursuing the Ph.D. degree in electronic and information engineering with Beijing Institute of Technology, Beijing, China. His research interests include electromagnetic inverse scattering imaging algorithms and antenna design. He won the Best Oral Presentation Award in the 2023 IEEE International Workshop on Electromagnetics: Applications and Student Innovation Competition (iWEM) held in Harbin.

HUI ZHANG received the B.Sc. degree from Northwest Polytechnique University, Xi'an, China, the M.Sc. degree from Concordia University, Montréal, QC, Canada, in 2002, and the Ph.D. degree from Montréal University, Montréal, in 2007. She was with Broadcom, Sunnyvale, CA, USA, as a Senior Principle Engineer. She is currently a Professor with Beihang University, Beijing, China. Her areas of interests include millimeter-wave transceiver development, mixed-signal IC, LNA, PA, and PLLs.

XIUZHU YE (Senior Member, IEEE) received the bachelor's degree in communication engineering from Harbin Institute of Technology, in 2008, and the Ph.D. degree in electrical engineering from the National University of Singapore (NUS), in 2012. She joined Department of Information and Electronics, Beijing Institute of Technology (BIT), in May 2019, as an Associate professor and the Ph.D. Director. Before joining BIT, she was an Assistant Professor with Beihang University. Before that, she did a postdoctoral research with the Department of Electrical and Computer Engineering, NUS, in May 2012. Her current research interests include inverse problems, biomedical imaging systems, security imaging systems, through wall imaging radar, and related machine learning algorithms. She has published more than 80 scientific articles in the related areas, including more than 20 articles in top journals. She also serves as the Youth Deputy Director with the EMC Branch; and a member of Council at Young Women Scientists Club, China Electronics Society.